J. Math. Study
doi: 10.4208/jms.v52n3.19.07

Vol. **52**, No. 3, pp. 341-358
September 2019

The Direct Robin Boundary Value Parabolic System of Time-Resolved Diffuse Optical Tomography with Fluorescence

Zakaria Belhachmi[1,*], Guillaume Dollé[2], Christophe Prud'homme[3] and Murielle Torregrossa[4]

[1] *Université Haute Alsace, LMIA EA 7499, 68093 Mulhouse, France,*
[2] *Université de Reims Champagne Ardenne, LMR FRE 2011, 51100 Reims, France,*
[3] *Université de Strasbourg, IRMA UMR 7501, 67084 Strasbourg, France,*
[4] *Université de Strasbourg, ICube UMR 7357, 67412 Illkirch, France.*

Received January 30, 2019; Accepted July 5, 2019

Abstract. We consider a system of parabolic PDEs with measure data modelling a problem of the time resolved diffuse optical tomography with a fluorescence term and Robin boundary conditions. We focus on the direct problem where the quantity of interest is the density of photons in the diffusion equations and which constitutes a major step to solve the inverse problem of identifiability and reconstruction of diffusion, absorption and concentration of the fluorescent markers. We study the problem under a variational form and its discretization with finite element method and we give some numerical simulation results for verification purpose as well as simulations with real data from a tomograph.

AMS subject classifications: 65N21, 65J22, 78A46

Key words: Tomography, scattering, fluorescence, contact, non-contact.

1 Introduction

We consider the Time-Resolved Diffuse Optical Tomography (TR-DOT) problem with fluorescence arising in the medical and biological imaging for soft tissues, small animal studies and noninvasive methods of tumor detection [1, 9, 13, 14]. The final goal in this imaging modalities is the reconstruction of physical parameters such as diffusion and absorption coefficients. While IRM and X-Ray tomography are usually of high resolution and deep penetration properties allowing exploring the object in-depth but with poor

*Corresponding author. *Email addresses:* zakaria.belhachmi@uha.fr (Z. Belhachmi), guillaume.dolle@univ-reims.fr (G. Dollé), christophe.prudhomme@math.unistra.fr (C. Prud'homme), m.torregrossa@unistra.fr (M. Torregrossa)

contrast, the optical tomography is very sensitive to the contrast but with poor resolution. In addition, the optical tomography is only efficient in thin regions close to the detectors. However, due to its cheap cost and noninvasive features, its recommended for some type of tumor (skin, breasts, neonatal imaging,...). In order to increase its efficiency, it is usually coupled with the use of fluorescent molecules which enhance the contrast in the tissues. The mathematical model of (TR-DOT) is a parabolic system with a memory term and measure data. In simple geometric setting (disk, cylinder) and assuming some regularity of the solutions, the mathematical study of the resulting problem follows from standard methods of the calculus of variations but in the general setting one has to use more technical and involved methods to solve the parabolic systems (e.g. approximation approach [2, 3, 12]). Moreover, there are two different experimental setting leading to two kind of data and measurements: the contact case where the detection and excitation fibers are set directly on the object under consideration and the non-contact case where they are not. This yields two mathematical models for which the governing equations are unchanged while the data and measurement terms are either Dirac masses on isolated points in the first case or Dirac masses on lines in 2D and surfaces in 3D configurations (any all cases sets of small dimension). The main goal in this article is to study such problems and to perform the numerical analysis as well as preliminary numerical simulations on both academic data for verification purpose in different implementation settings (Matlab and Feel++ softwares) as well as real data from an experimental tomograph of Icube Laboratory (university of Strasbourg). The diffusion approximation for the optical tomography called time resolved diffuse optical tomography, DOT-TR, is widely used and documented in medical and biological imaging, we refer the reader to the review of S. Arridge and the references therein [1]. In contrast, only a few references are available for the fluorescent case and to our knowledge almost no mathematical and numerical study have been done yet. We refer to [4] for the physical model and related references on the subject. The paper is organized as follows. The Section 2 proposes a study for the well-posedness of the coupled system of equations for the contact case, Section 2.1 and the non-contact case, Section 2.2. Some mathematical preliminaries are introduced, the weak formulations and some theoretical results are stated. In Section 3, we set the discrete framework with emphasis on the methods to handle the fluorescence source term which can be seen as a memory source term, but can also be treated without explicit integration (Duhamel formulae) by introducing an Ordinary Differential Equations (ODE) to the initial system. Finally, two convergence results are given depending on the chosen source term for the contact and the non-contact mode.

2 Mathematical model-Weak formulations

In this section, we briefly give some mathematical tools and results on the models under consideration. We derive also the associated weak formulations on which our discretization is based. We refer for details to [4]. We call tomograph an experimental device which

consists of $N_s \in \mathbb{N}$ optical fibers, acting as light sources and detectors, and placed on a ring and surrounding for instance a phantom object or a small animal to be imaged by the tomograph. Let Ω be a bounded domain of $\mathbb{R}^d$ ($d=2$ or 3) and $T>0$. We denote $\ell \in \{x,m\}$ the subscript respectively for the diffusion and fluorescence excitation wavelength. The system of equations that describes the tomograph setup as a sequence of diffusion problems within each fiber and through Ω is written: $1 \le k \le N_s$,

$$\begin{cases} -\nabla\cdot(\kappa_x \nabla \phi_x^k) + c_e \mu_{a,x} \phi_x^k + \dfrac{\partial \phi_x^k}{\partial t} = q_x^k & \text{on } \Omega \times (0,T), \\ -\nabla\cdot(\kappa_m \nabla \phi_m^k) + c_e \mu_{a,m} \phi_m^k + \dfrac{\partial \phi_m^k}{\partial t} = \gamma q_m^k & \text{on } \Omega \times (0,T), \\ \phi_x^k + 2\mathrm{A}\kappa_x \dfrac{\partial \phi_x^k}{\partial \boldsymbol{n}} = 0 & \text{on } \partial\Omega \times (0,T), \\ \phi_m^k + 2\mathrm{A}\kappa_m \dfrac{\partial \phi_m^k}{\partial \boldsymbol{n}} = 0 & \text{on } \partial\Omega \times (0,T), \\ \phi_x^k(0,\cdot) = 0, \qquad \phi_m^k(0,\cdot) = 0, \end{cases} \tag{2.1}$$

where the wavelenght dependent quantities denote respectively ϕ_ℓ^k the photon density, $\mu_{a,\ell}$ the absorption coefficients, and κ_ℓ the diffusion coefficients given by

$$\kappa_\ell = \frac{c_e}{(3(\mu_{a,\ell} + \mu'_{s,\ell}))}, \tag{2.2}$$

where $\mu'_{s,\ell}$ is the scattering coefficients. The fluorophore coefficient $\gamma = \eta\sigma\xi$ depends on the flurorophor concentration ξ, the fluorophore molar extinguishing coefficient σ and the fluorophore yield η. Finally, τ corresponds to the fluorophore average lifetime and A is a given constant (see [4]). There are two approaches to handle the source terms q_k^x, the contact mode where q_k^x is a Dirac mass on a single point in Ω or the non contact mode where q_k^x is a Dirac mass supported on low dimensional set, a line when d=2 and a surface when $d=3$. Our contributions in this modelling part is to consider systematically and rigourously these two models and to compare them both theoretically and numerically. We set

$$q_x^k = \begin{cases} \delta_{x_0^k}(\mathbf{x})\delta(t_0) & \text{(contact case)}, \\ \delta_{\Sigma_0^k}(\mathbf{x})\delta(t_0) & \text{(non contact case)}. \end{cases} \tag{2.3}$$

The fluorescence source term q_m^k in this modelling is a response at the wavelength λ_m and takes the form of convolution (in time) of the photon density at λ_x with an exponential kernel times a fluophor concentration. This source term modelizes the fluorophore excitation photons generated once the diffusion photons hit the biomarker

$$q_m^k(\mathbf{x},t) = \frac{1}{\tau}\int_0^t \phi_x^k(\mathbf{x},s) e^{(\frac{t-s}{\tau})} ds. \tag{2.4}$$

Remark 2.1. We assume null initial conditions which means that we neglect the mean free path otherwise we should have to take into account a direction information for the particles transport.

We denote by $Q=\Omega\times(0,T)$ the time-space domain and by $M(\overline{\Omega})=C(\overline{\Omega})'$, the usual bounded Radon measures space (i.e. dual of the space of the continuous functions equipped with its usual norm). We consider the coupled system of parabolic equations (2.1) and we will drop the index $k\in[1,N_s]$ in this section for brevity. We assume there exists two constants κ_0, κ_1 such that: for $\ell=\{x,m\}$

$$\begin{cases}\kappa_\ell,\mu_{a,\ell}\in L^\infty(\Omega), & \mu_{a,\ell}\geq 0,\\ 0<\kappa_0\leq\kappa_x,\kappa_m\leq\kappa_1.\end{cases} \tag{2.5}$$

We have to distinguish the two cases: contact model where the datum q_x is only in $H^{-s}(\Omega)$, $s\geq 2$ and the non contact model where it belongs to the dual space $(H^1(\Omega))'$.

Remark 2.2. Note that in the case of smooth coefficients $\kappa_x,\mu_{a,x}$ (e.g. Hölder continuous), and simple geometries, the first equation may be solved with the fondamental solution method and the second one is then uncoupled from the first one and with a regular right-hand side, thus fit under the framework of the standard variational theory [7]. In the general case (2.5), we have to consider a more general setting of parabolic equations with measure data [2,3].

2.1 The contact case

Let $\ell=\{x,m\}$, $q_x\in M(\overline{\Omega})$. We recall that in our setting we have $q_x=\delta_{x_0}$, with $x_0\in\Omega$. The theory of parabolic equations with measure data show that weak solutions or only defined in the spaces $W_q=L^q(0,T;W^{1,q}(\Omega))$ for any $1\leq q<\frac{d+2}{d+1}$ (e.g. [3]), loosely speaking one wants the tests functions to be in $H^1(\Omega)\cap C(\overline{\Omega})$). In the case of our system the first equation fit under this general framework, whereas the second equation possesses more regularity for the right-hand side term and solutions are searched in classical spaces for second order parabolic equations. More precisely, let $V^c=\cup_{q>\frac{d}{d-1}}W^{1,q}(\Omega)$, $d\geq 2$. In order to write the weak formulation of the system (2.1), we consider each equation:

(i) Find $\phi_x(t)\in\cap_{p<\frac{d}{d-1}}W^{1,p}(\Omega)$, and $\frac{\partial\phi_x}{\partial t}\in\cap_{p<\frac{d}{d-1}}W^{-1,p}(\Omega)$ for a.e $t>0$

$$\int_\Omega\kappa_x\nabla\phi_x\nabla v+\int_\Omega c_e\mu_a\phi_x v+\int_{\partial\Omega}\frac{1}{2A}\phi_x v+\int_\Omega\frac{\partial\phi_x}{\partial t}v=(q_x,v)\quad\forall v\in V^c. \tag{2.6}$$

Note that v is continuous, and (q_x,v) is $v(x_0)$. The integral $\int_\Omega\frac{\partial\phi_x}{\partial t}v$ is to be understood in the duality sense ($\frac{\partial\phi_x}{\partial t}\in W^{-1,p}(\Omega)$ for $p<\frac{d}{d-1}$, and $v\in V^c$ a.e $t>0$).

(ii) the source term q_m depends on ϕ_x. We look for a solution $\phi_m\in H^1(\Omega)$ more regular than ϕ_x such that

$$\int_\Omega\kappa_m\nabla\phi_m\nabla v+\int_\Omega c_e\phi_m\mu_{a,m}v+\int_{\partial\Omega}\frac{1}{2A}\phi_m v+\int_\Omega\frac{\partial\phi_m}{\partial t}v=\langle\gamma q_m,v\rangle_{H^{1\prime}(\Omega),H^1(\Omega)}. \tag{2.7}$$

As a detailed mathematical analysis of the problem is beyond the scope of this article, we only state the well posedness result in the contact case without proof and we refer the interested reader to [4] for details.

Theorem 2.1. *Under the hypothesis* (2.5) *for any* $1 \leq q < \frac{d+2}{d+1}$ *there exists a solution* (ϕ_x, ϕ_m) *to the system* (2.1), *such that* $\phi_x \in W_q$, *and* ϕ_m *is such that:* $\phi_m \in L^2(0,T;H^1(\Omega)) \cap C([0,T];L^2(\Omega))$, $\phi_m' \in L^2(0,T;(H^1(\Omega))')$, *If* $d=2$, *and* $\phi_m, \phi_m' \in L^p(0,T,W^{1,p}(\Omega))$ $(p \leq \frac{3}{2})$, *If* $d=3$.

Note that the solutions given by the theorem are such that the initial conditions $\phi_\ell(0,.) = 0$, $\ell = \{x,m\}$ are taken in the classical sense since $\phi_m(t)$ is continuous and ϕ_x belongs to $C([0,T];H^{-s}(\Omega))$ for large $s>0$ [3].

Remark 2.3. The theorem suggests, due to the different regularity properties for ϕ_x and ϕ_m, that the discretization errors will be better for ϕ_m, thus it may be advantageous to use different finite elements for each variable [4].

2.2 The non-contact case

Let us consider the non contact case $q_{x_0} = \delta_{\Sigma_0} \in H^{1\prime}(\Omega)$ when Σ_0 is a closed surface in Ω, as it may be checked that

$$< q_{x_0}, v >_{H^{1\prime},H^1} = \int_{\Sigma_0} v d\sigma, \quad \forall v \in H^1(\Omega). \tag{2.8}$$

Remark 2.4. If Σ_0 is an open surface, we have to modify the functional setting but a part from technicalities the study follows the same lines. We focus on the case of a closed surface for brevity.

We set $V = H^1(\Omega)$. The weak formulation in this case is given by:
(i) Find $\phi_x(t) \in V$, and $\frac{\partial \phi_x}{\partial t} \in V'$ for a.e $t>0$

$$\int_\Omega \kappa_x \nabla \phi_x \nabla v + \int_\Omega c_e \mu_a v + \int_{\partial\Omega} \frac{1}{2A} \phi_x v + \int_\Omega \frac{\partial \phi_x}{\partial t} v = (q_x, v)_{V',V} \quad \forall v \in V. \tag{2.9}$$

Note that (q_x, v) is the integral $\int_\Sigma v d\sigma$.

(ii) the source term q_m depends on ϕ_x, we therefore search a solution $\phi_m \in V$, with $\frac{\partial \phi_m}{\partial t} \in L^2(\Omega)$ such that

$$\int_\Omega \kappa_m \nabla \phi_m \nabla v + \int_\Omega c_e \mu_{a,m} v + \int_{\partial\Omega} \frac{1}{2A} \phi_m v + \int_\Omega \frac{\partial \phi_m}{\partial t} v = \langle \gamma q_m, v \rangle_{V',V}. \tag{2.10}$$

Note that the integral $\int_\Omega \frac{\partial \phi_m}{\partial t} v$ is to be understood in the duality sense V', V.

Remark 2.5. Note that we take $\mu_{a,x}$ nonnegative which is too stringent. However, if $\mu_{a,x} \equiv 0$ on $w \subset \Omega$, then we have to modify the functional setting to ensure the Poincar-Wirtinger inequality and the results hold.

We refer to [4] for the proof of the following theorem.

Theorem 2.2. *Under the hypothesis* (2.5) *there exists a unique solution* (ϕ_x,ϕ_m) *to the system* (2.1), *such that* $\phi_x\in L^2(0,T;H)\cap C(0,T;V')$, *and* $\phi_m\in L^2(0,T;V)\cap C(0,T;H)$, $\frac{\partial\phi_m}{\partial t}\in L^2(0,T;V')$.

We note that when the coefficients κ_ℓ,μ_ℓ, $\ell=\{x,m\}$ are regular, say $W^{1,\infty}(\Omega)$, the solution $\phi_m\in L^2(0,T;H^2(\Omega)\cap V)\cap C([0,T];V)$ and $\frac{\partial\phi_m}{\partial t}\in L^2(0,T;H)$ (see [6,7]). In all cases, the solutions satisfy the initial conditions in the classical sense and the Robin boundary condition in the usual sense of traces.

3 Discrete formulations

3.1 Semi-discrete formulation

In the following section, we drop the index k for simplicity. We discretize in time such that $t_n=n\Delta t$. We denote $\boldsymbol{\phi}^{(n)}(\boldsymbol{x})=\boldsymbol{\phi}(\boldsymbol{x},t_n)$ the solution of the system (2.1) and $\mathbf{q}^{(n)}=\mathbf{q}(\phi_x;\boldsymbol{x},t_n)$ the source term. We discretize the time dependent term using a backward Euler scheme in time. Thus, the semi-discrete formulation reads

$$\begin{aligned}&\int_\Omega\left(\boldsymbol{\kappa}\nabla\boldsymbol{\phi}^{(n+1)}:\nabla\boldsymbol{v}+c_e\boldsymbol{\mu}_a\boldsymbol{\phi}^{(n+1)}\boldsymbol{v}\right)+\int_{\partial\Omega}\frac{1}{2\mathrm{A}}\boldsymbol{\phi}^{(n+1)}\boldsymbol{v}+\int_\Omega\frac{\boldsymbol{\phi}^{(n+1)}}{\Delta t}\boldsymbol{v}\\&=\int_\Omega\mathbf{q}^{(n+1)}\boldsymbol{v}+\int_\Omega\frac{\boldsymbol{\phi}^{(n)}}{\Delta t}\boldsymbol{v}.\end{aligned}\tag{3.1}$$

We must yet see how to deal with the source term for the fluorescence q_m. We can use the Chasle relation to rewrite the integral such that

$$q_m^{(n+1)}=\frac{1}{\tau}\int_0^{t_{n+1}}\phi_x(\boldsymbol{x},s)e^{(\frac{t_{n+1}-s}{\tau})}ds=f(t_{n+1})\left(B_n(\boldsymbol{x})+R_n(\boldsymbol{x})\right)\tag{3.2}$$

with $f(t)=\frac{1}{\tau}e^{\frac{t}{\tau}}$ and $B_n(\boldsymbol{x})$ a memory term defined such that

$$B_n(\boldsymbol{x})=\int_0^{t_n}\phi_x(\boldsymbol{x},s)e^{-\frac{s}{\tau}}ds,\tag{3.3}$$

stored and $R_n(\boldsymbol{x})$ a remain term to compute such that

$$R_n(\boldsymbol{x})=\int_{t_n}^{t_{n+1}}\phi_x(\boldsymbol{x},s)e^{-\frac{s}{\tau}}ds.\tag{3.4}$$

Therefore we just have to compute the integral $R_n(\boldsymbol{x})$ knowing that $\phi_x(\boldsymbol{x},t)$ is first order polynomial of the time on the restricted interval $[t_n,t_{n+1}]$ and also that its borned values are fixed.

$$\phi_x(\boldsymbol{x},t)=a(\boldsymbol{x})t+b(\boldsymbol{x}),\tag{3.5}$$

where the coefficients a and b are respectively,

$$a(\boldsymbol{x})=\frac{\phi_x^{(n+1)}(\boldsymbol{x})-\phi_x^{(n)}(\boldsymbol{x})}{\Delta t},\quad b(\boldsymbol{x})=\phi_x^{(n+1)}-a(\boldsymbol{x})t_{n+1}.\tag{3.6}$$

We integrate by parts the integral (3.4),

$$\begin{aligned} R_n(\boldsymbol{x}) &= \left[-\tau\phi_x(\boldsymbol{x},s)e^{-\frac{s}{\tau}}\right]_{t_n}^{t_{n+1}} + \tau\int_{t_n}^{t_{n+1}} \phi_x'(\boldsymbol{x},s)e^{-\frac{s}{\tau}}ds \\ &= -a(\boldsymbol{x})\tau\Delta t(n\omega_1+1) - \tau(b(\boldsymbol{x})+a(\boldsymbol{x})\tau)\omega_1, \end{aligned} \tag{3.7}$$

where the coefficients w_1 reads

$$\omega_1 = 1-e^{\Delta t/\tau}. \tag{3.8}$$

Now, if we replace $a(\boldsymbol{x})$ and $b(\boldsymbol{x})$ with their values (3.6), the remaining term can be expressed such that

$$R_n(\boldsymbol{x}) = C_1\phi_x^{(n+1)} + C_2\phi_x^{(n)}, \tag{3.9}$$

where the coefficients C_1 and C_2 are,

$$C_1 = \tau\left(-1-\frac{\tau\omega_1}{\Delta t}\right), \qquad C_2 = \tau\left(1+\left(\frac{\tau}{\Delta t}-1\right)\omega_1\right). \tag{3.10}$$

Using Chasle relation again in Section 3.3, the recursive formula for $B_n(\boldsymbol{x})$ can be established

$$B_n(\boldsymbol{x}) = B_{n-1}(\boldsymbol{x}) + R_{n-1}(\boldsymbol{x}). \tag{3.11}$$

In particular we have $B_0 = 0$ and R_0 defined such that

$$R_0(\boldsymbol{x}) = \phi_x^{(0)}\tau(1-\omega_1) - \tau\phi_x^{(1)}. \tag{3.12}$$

Finally, we obtain the semi-discrete formulation

$$\begin{aligned} &\int_\Omega (\kappa\nabla\boldsymbol{\phi}^{(n+1)} : \nabla\boldsymbol{v} + c_e\mu_a\boldsymbol{\phi}^{(n+1)}\cdot\boldsymbol{v}) + \int_{\partial\Omega}\frac{1}{2A}\boldsymbol{\phi}^{(n+1)}\cdot\boldsymbol{v} + \int_\Omega \frac{\boldsymbol{\phi}^{(n+1)}}{\Delta_t}\cdot\boldsymbol{v} \\ &= \int_\Omega \begin{pmatrix} q_x^{(n+1)} \\ \gamma(\boldsymbol{x})f^{(n+1)}B_n(\boldsymbol{x}) \end{pmatrix}\cdot\boldsymbol{v} + \int_\Omega \begin{pmatrix} 0 \\ \gamma(\boldsymbol{x})f^{(n+1)}R_n(\boldsymbol{x}) \end{pmatrix}\cdot\boldsymbol{v} + \int_\Omega \frac{\boldsymbol{\phi}^{(n)}}{\Delta_t}\cdot\boldsymbol{v}. \end{aligned} \tag{3.13}$$

Remark 3.1. For $n>0$, the term $B_n(\boldsymbol{x})$ is known and has to be updated for each time step.

Second method Instead of handling the memory term in the fluorescence equation, a second method consists in introducing the ODE on the fluorescence source term q_m detailed in Section 2.1 in the original model. Thus, a new degenerated problem is considered consisting of (2.1) with, in addition the following equation

$$\begin{cases} (2.1), \\ q_m'^k - \frac{1}{\tau}q_m^k = \frac{1}{\tau}\phi_x^k \qquad \text{on } \Omega\times(0,T). \end{cases} \tag{3.14}$$

Considering equation (3.14), we convert a memory cost for a computational cost, but more efficient by solving the new ODE equation (3.14) explicitly. A possible advantage is for different time grids. As the solution for the fluorescence problem depends on the regularity of ϕ_x, we might choose a coarse grid for the fluorescence and adapt the ODE scheme (e.g high order Runge Kutta (RK method) to regularize the solution with the aim to reduce the computational cost of the global system.

3.2 Full Discrete formulation

We now turn to the Galerkin approximation of the semi-discrete problem (3.13). The space discretization may vary depending on the contact or non-contact case follow Section 2 analysis. Let $Z_h = V_h \times W_h \subset [H^1(\Omega)]^2$ the discrete spaces of the problem (3.13), V_h associated the diffusion and W_h associated to the fluorescence equations respectively. The subscript h denotes the space discretization step. Let $\mathcal{T}_h$ be a space grid for the domain Ω. Let N_i denotes the mesh vertices of $\mathcal{T}_h$ with $i \in [1, N_h]$. We introduce a vectorial basis $\{\boldsymbol{\varphi}_j\}$ for Z_h defined by

$$\boldsymbol{\varphi}_j(N_i) = \left\{ \varphi_j^k(N_i) \,|\, k \in \{x, m\} \right\}, \tag{3.15}$$

the basis function of the space V_h and W_h for $k = x$ and $k = m$ respectively, such that

$$\varphi_j^k(N_i) = \delta_{i,j} = \begin{cases} 0 & i \neq j, \\ 1 & i = j, \end{cases} \quad i,j = 1,\ldots,N_h. \tag{3.16}$$

We introduce the Galerkin approximation $\boldsymbol{\phi}_h^{(n)} = \{\boldsymbol{\phi}_x^{(n)}, \boldsymbol{\phi}_m^{(n)}\} \in [V_h]^2$ defined for each $t \approx t_n$ with $n > 0$ of (3.13).

$$\boldsymbol{\phi}_h^{(n)}(\boldsymbol{x}) = \sum_{j=1}^{N_h} \phi_j^n \boldsymbol{\varphi}_j(\boldsymbol{x}), \tag{3.17}$$

and we denote $\boldsymbol{\phi}_h^{(n)} = \boldsymbol{\phi}_h^{(n)}(\boldsymbol{x})$ for brevity. The semi-discrete formulation (3.13) reads

$$\begin{aligned} &\int_\Omega (\kappa \nabla \boldsymbol{\phi}_h^{(n+1)} : \nabla \boldsymbol{v}_h + c_e \mu_a \boldsymbol{\phi}_h^{(n+1)} \cdot \boldsymbol{v}_h) + \int_{\partial\Omega} \frac{1}{2A} \boldsymbol{\phi}_h^{(n+1)} \cdot \boldsymbol{v}_h + \int_\Omega \frac{\boldsymbol{\phi}_h^{(n+1)}}{\Delta_t} \cdot \boldsymbol{v}_h \\ &= \int_\Omega \begin{pmatrix} q_x \\ \gamma(\boldsymbol{x}) f^{(n+1)} B_n(\boldsymbol{x}) \end{pmatrix} \cdot \boldsymbol{v}_h + \int_\Omega \begin{pmatrix} 0 \\ \gamma(\boldsymbol{x}) f^{(n+1)} R_n(\boldsymbol{x}) \end{pmatrix} \cdot \boldsymbol{v}_h + \int_\Omega \frac{\boldsymbol{\phi}_h^{(n)}}{\Delta_t} \cdot \boldsymbol{v}_h. \end{aligned} \tag{3.18}$$

We introduce the Galerkin approximation $q_{x,h}^{(n)}$ for the diffusion source term such that for the contact case (i), we have

$$q_{x,h}^{(n)} = \begin{cases} \sum_{j=1}^{N_h} \delta_{h,j} \varphi_j(x) & n = 0, \\ 0 & n > 0, \end{cases} \tag{3.19}$$

such that

$$\delta_{h,j} = \begin{cases} 1 & j = j_0 \,(x = x_0), \\ 0 & \text{else}, \end{cases} \tag{3.20}$$

and for the non contact case, we have

$$q_{x,h}^{(n)} = \begin{cases} \sum_{i=1}^{N_h} \delta_h \varphi_j(x_{\Sigma_0}) & n = 0, \\ 0 & n > 0. \end{cases} \tag{3.21}$$

The remainder term written in the finite element basis is

$$R_n = C_1 \sum_{j=1}^{N_h} \phi_j^{(n+1)} \varphi_j + C_2 \sum_{j=1}^{N_h} \phi_j^{(n)} \varphi_j, \tag{3.22}$$

then we may write Then, setting

$$a_{i,j} = \int_\Omega \boldsymbol{\kappa} \nabla \boldsymbol{\varphi}_j : \nabla \boldsymbol{\varphi}_i, \qquad b_{i,j} = \int_\Omega \boldsymbol{\mu}_a \boldsymbol{\varphi}_j \boldsymbol{\varphi}_i, \tag{3.23a}$$

$$m_{i,j} = \int_\Omega \boldsymbol{\varphi}_j \boldsymbol{\varphi}_i, \qquad f_{i,j} = \int_\Omega \gamma(\boldsymbol{x}) \begin{pmatrix} 0 \\ \varphi_j \end{pmatrix} \boldsymbol{\varphi}_i. \tag{3.23b}$$

We obtain the algebraic form

$$A\boldsymbol{\Phi}^{(n+1)} + c_e B\boldsymbol{\Phi}^{(n+1)} + M\left(\frac{1}{2A} + \frac{1}{\Delta_t}\right)\boldsymbol{\Phi}^{(n+1)} - C_1 F\boldsymbol{\Phi}^{(n+1)} = \mathcal{Q}^n. \tag{3.24}$$

3.3 Convergence results

We now give a convergence result depending on the type of source q_x considered. The contact case result is based on the proof of [11] whereas the non-contact one is based on [5] results. For the non-contact case, we are taking into account that the surface for the δ-Dirac source can be taken on a different mesh from the domain Ω introducing an interpolation error for the worst scenario.

Contact case We give the error bound for general finite elements approximation of degree m, since we implemented various type conforming finite elements. We place ourselves under the same hypothesis as [11]. Let us denote Ω the whole domain and $\mathcal{T}_h$ a triangulation on $\Omega \in \mathbb{R}^d$ with $d > 0$ the dimension. We denote V the Sobolev completion of $H^m(\Omega)$. We recall the result of [11]. Let V be a Hilbert space associated to the variational formulation of an elliptic problem with right-hand side a Dirac measure δ_{x_0}, $x_0 \in \Omega$, for an operator of order $2m$, $m \geq 1$ (V is the completion of smooth functions in the Sobolev space $H^m(\Omega)$). Let S^h be a finite element subspace of V. We say that S^h approximates to degree k in V if for each smooth u in V:

$$\inf_{v \in S^h} \|u - v\|_{H^s(\Omega)} \leq C(x_0) h^{k-s} \|u\|_k, \quad \text{for } 0 \leq s \leq m. \tag{3.25}$$

Typically, for $m = 1$ the degree $k = \ell + 1$, where ℓ is the polynomial degree in $S^h = V_h$. Then we have the theorem (see [11]).

Theorem 3.1. *If ϕ_x solves* (2.1) *in the sense of distributions for $q_x = \delta_{x_0}$ and $\phi_{x,h}$ is the solution to the associated variational problem, then*

$$\|\phi_x - \phi_{x,h}\|_{H^s} \leq C(x_0) h^{2m - \frac{d}{2} - s} \quad \text{for } 2m - k \leq s < 2m - \frac{d}{2}, \tag{3.26}$$

if $k \geq 2m$ then $C(x_0)$ goes to infinity as x_0 approaches $\partial\Omega$.

In particular, according to (3.25), we have for $d=2$, $m=1$ and $\ell=1$ the convergence rate $O(h^{1-s})$ for $0\leq s\leq 1$. With $d=3$, we obtain $O(h^{\frac{1}{2}-s})$ for $0\leq s\leq \frac{1}{2}$.

Remark 3.2. In our case, the distance $d(x_0,\partial\Omega)$ corresponds to the mean free path which is the medium length of a path covered by a photon (or particle) between subsequent impacts. In practice, this distance is taken equal to the inverse of the reduced scattering coefficient $d(x_0,\partial\Omega)=\frac{1}{\mu_s'}$. Note that as x_0 goes to $\partial\Omega$ the constant $C(x_0)$ goes $+\infty$ [11].

Non contact case In the following section, an error estimate is proposed for our special source term of Dirac type.

In [5] consider a Laplace equation in 2D for which they derive an error estimate. We follow the same approach that we extend to he 3D case. To cover the cases that we have implemented and for sake of completeness we give the results even for Σ an open curve and with different meshes on Ω and Σ (not compatible in general).

The method consists in approximating the source term by a sum of Dirac masses for Σ_0. To handle the right hand side $q_x(\boldsymbol{x},t)$, we denote $q_(x)=\delta_{\Sigma_0}$ and Σ_0 Then for any $v\in V\subset H^1(\Omega)$, we have

$$<q_x,v>_{H^{-1},H^1}=<\delta_{\Sigma_0},v>_{H^{-1},H^1}=\int_{\Sigma_0} v. \tag{3.27}$$

Given a triangulation $\mathcal{T}_h$ of Ω we introduce $\mathcal{T}_{\tilde{h}}$ a discretization of Σ_0 of $d-1$ dimension. One denotes $\mathcal{E}_h$ the interior edges of the mesh $\mathcal{T}_h$. We assume that $\mathcal{T}_{\tilde{h}}$ is not a submesh of $\mathcal{E}_h$ (Note that if $\mathcal{T}_{\tilde{h}}$ is a submesh of $\mathcal{E}_h$, then following calculations are simpler since it is not necessary to interpolate between meshes). Recall that V_h is the P_1 conforming finite element space defined by

$$V_h=\Big\{v_h\in C^0(\overline{\Omega}),v_{h|K}\,\text{affine},\quad \forall K\in\mathcal{T}_h\Big\}. \tag{3.28}$$

Lemma 3.1. *Let $D\in\mathbb{R}^d$ with $d=1,2$ be a smooth domain. Let Σ_0 an open curve, Σ_e a smooth curve such that $\Sigma_0\cap\Sigma_e=\emptyset$ and $\partial D=\overline{\Sigma}_0\cup\overline{\Sigma}_e$. Let denote $\tilde{h}>0$ and $\mathcal{T}_{\tilde{h}}$ a family of quasi-uniform d-dimensionnal triangulations of Σ_0 with Σ_i, $1<i<N$ the subintervals. The quasi-uniformity expresses*

$$c\tilde{h}^d\leq|\Sigma_i|\leq C\tilde{h}^d,\quad \textit{with } 0<c<C. \tag{3.29}$$

We consider a set of points in the subsurfaces $x_i\in\Sigma_i$. For $v\in H^1(\Sigma_i)$, the piecewise constant interpolant reads

$$v_{\tilde{h}}=\sum_{i=1}^{N} v(x_i)\mathbb{1}_{\Sigma_i}. \tag{3.30}$$

Then for $0\leq s<1/2$, we have

$$\|v-v_{\tilde{h}}\|_{H^s}\leq C\tilde{h}^{1-s}|v|_1, \tag{3.31}$$

with $|v|_1$ the H^1 seminorm and the associated usual Sobolev norm

$$\|w\|_{H^s}=\left(\int_{\Sigma_0}|w|^2\right)^{1/2}+\left(\int_{\Sigma_0}\int_{\Sigma_0}\frac{|w(\boldsymbol{y})-w(\boldsymbol{x})|^2}{\|\boldsymbol{y}-\boldsymbol{x}\|^{2(s+\frac{d}{2})}}\right)^{1/2},\quad 0\leq s<1/2. \tag{3.32}$$

Proof. For d=1 the proof follows [5]. For d=2, we have to find a majoration of (3.32). We first split the second term in the Sobolev norm (3.32) to treat, for the case $\boldsymbol{y}-\boldsymbol{x}=0$, the diagonal *(i)* and the non-diagonal terms *(ii)*, then find a majoration for the first L_2 norm term *(iii)*. We denote $w_{\tilde{h}}=v-v_{\tilde{h}}$ now and hereafter.

(i) For the diagonal terms, using the Taylor formula then applying the Cauchy-Schwarz inequality, we find

$$\begin{aligned}\sum_{i=1}^{N}\int_{\Sigma_i}\int_{\Sigma_i}\frac{|v(\boldsymbol{y})-v(\boldsymbol{x})|^2}{\|\boldsymbol{y}-\boldsymbol{x}\|^{2(s+\frac{d}{2})}}&\leq\sum_{i=1}^{N}\int_{\Sigma_i}\int_{\Sigma_i}\left(\int_0^1|Dv(\boldsymbol{x}+t\boldsymbol{\nu})|^2dt\right)\frac{|\boldsymbol{\nu}|^2}{|\boldsymbol{\nu}|^{2(s+\frac{d}{2})}}\\&\leq\sum_{i=1}^{N}\left(\int_{\Sigma_i}|Dv(\boldsymbol{z})|^2dz\right)\int_{\Sigma_i}\int_{\Sigma_i}|\boldsymbol{\nu}|^{-2(s+\frac{d}{2})+2}.\end{aligned} \tag{3.33}$$

For the last double integral, we perform a majoration on $\Sigma_i=I_1\times I_2$, For d=1 the majoration is given in [5]. For d=2, let (x_j,y_j) for $1\leq j\leq 2$ be a couple of points in Σ_i,

$$\int_{\Sigma_i}\int_{\Sigma_i}|\boldsymbol{\nu}|^{-2s}=\int_{\Sigma_i}\left(\int_{I_1}\int_{I_2}|(y_1-x_1)^2+(y_2-x_2)^2|^{-s}\right), \tag{3.34}$$

we note that $|w|^\alpha$ is convex for $\alpha<0$. Thus for $\theta\in[0,1]$ convexity writes as

$$|\theta a+(1-\theta)b|^\alpha\leq\theta|a|^\alpha+(1-\theta)|b|^\alpha \tag{3.35}$$

and choosing coefficients

$$a=\frac{(y_1-x_1)^2}{\theta},\qquad b=\frac{(y_2-x_2)^2}{(1-\theta)} \tag{3.36}$$

there exists $C_\theta>0$

$$|(y_1-x_1)^2+(y_2-x_2)^2|^\alpha\leq C_\theta|y_1-x_1|^{2\alpha}+C_\theta|y_2-x_2|^{2\alpha}. \tag{3.37}$$

For $\theta=\frac{1}{2}$, the constant is $C_0=\frac{1}{2^{1-\alpha}}$. For $\alpha=-s$ and going back to (3.34) one has the following majoration

$$\int_{\Sigma_i}\int_{\Sigma_i}|\boldsymbol{\nu}|^{-2s}\leq C_0\tilde{h}^2\int_{I_1}\int_{I_1}|y_1-x_1|^{-2s}+C_0\tilde{h}^2\int_{I_2}\int_{I_2}|y_2-x_2|^{-2s}. \tag{3.38}$$

For the last integral of (3.38) denoted I, let consider the following mapping

$$\begin{aligned} \varphi_i :\ \Sigma_i = I_1 \times I_2 &\longrightarrow [0,\tilde{h}] \times [0,\tilde{h}], \\ (x,y) &\longrightarrow \varphi_i(x,y) \end{aligned} \tag{3.39}$$

and J_φ the associated jacobian such that $\det(J_\varphi) \leq \tilde{h}^2$. Then the last integral of (3.38) can be calculated,

$$I = \int_0^{\tilde{h}} \int_0^{\tilde{h}} |y-x|^{-2s} \det(|J_\varphi|)^{-1} dxdy = \frac{2\tilde{h}^{-2s}}{(1-2s)(2-2s)}. \tag{3.40}$$

Thus, a majoration of (3.38) reads

$$\int_{\Sigma_i} \int_{\Sigma_i} |\boldsymbol{\nu}|^{-2s} \leq \frac{\tilde{h}^{2-2s}}{2^{s-1}(1-2s)(2-2s)}. \tag{3.41}$$

Then back to (3.33), we obtain the majoration

$$\sum_{i=1}^{N} \int_{\Sigma_i} \int_{\Sigma_i} \frac{|v(\boldsymbol{y}) - v(\boldsymbol{x})|^2}{\|\boldsymbol{y}-\boldsymbol{x}\|^{2(s+\frac{d}{2})}} \leq C_1 \tilde{h}^{2-2s} \left(\int_{\Sigma_0} |Dv(\boldsymbol{z})|^2 dz \right) \tag{3.42}$$

with a constant $C_1 = \frac{2^{1-s}}{(1-2s)(2-2s)}$.

(ii) Similarly, a majoration can be determined for the non diagonal term in the second term of (3.32). Relying on the Cauchy-Schwartz inequality and (3.41), we have

$$\begin{aligned} &\sum_{i=1}^{N} \sum_{j=1, j\neq i}^{N} \int_{\Sigma_i} \int_{\Sigma_j} \frac{|w_{\tilde{h}}(\boldsymbol{y}) - w_{\tilde{h}}(\boldsymbol{x})|^2}{\|\boldsymbol{y}-\boldsymbol{x}\|^{2(s+\frac{d}{2})}} \leq 4 \sum_{i=0}^{N} \sum_{j=0, j\neq i}^{N} \int_{\Sigma_i} \int_{\Sigma_j} \frac{|w_{\tilde{h}}(\boldsymbol{x})|^2}{|w|^{2s+2}} \\ \leq & 4 \sum_{i=1}^{N} \sum_{j=1, j\neq i}^{N} \int_{\Sigma_i} \int_{\Sigma_j} \left(\int_0^1 |Dv(\boldsymbol{z})|^2 dz \right) |\boldsymbol{\nu}|^{-2s} \\ \leq & C_2 \tilde{h}^{2-2s} \left(\int_{\Sigma_0} |Dv(\boldsymbol{z})|^2 dz \right) \end{aligned} \tag{3.43}$$

with a constant $C_2 = \frac{2^{3-s}}{(1-2s)(2-2s)}$.

As a consequence, the majoration for the double integral term in the Sobolev norm (3.32) reads

$$\left(\int_{\Sigma_0} \int_{\Sigma_0} \frac{|w(\boldsymbol{y}) - w(\boldsymbol{x})|^2}{\|\boldsymbol{y}-\boldsymbol{x}\|^{2(s+\frac{d}{2})}} \right)^{1/2} \leq C_3 \tilde{h}^{2-2s} |v|^2_{1,\Sigma_0} \tag{3.44}$$

with a constant $C_3 = C_1 + C_2 = \frac{5.2^{1-s}}{(1-s)(2-s)}$.

(iii) For the L_2 norm, using again Cauchy-Schwartz inequality, we deduce

$$\int_{\Sigma_0}|w_{\tilde{h}}|^2=\sum_{i=1}^{N}\int_{\Sigma_i}|w_h|^2$$

$$\leq\sum_{i=1}^{N}\left(\int_{\Sigma_i}|Dv(z)|^2dz\right)\int_{\Sigma_i}|\nu|^2\leq C_4\tilde{h}^2|v|^2_{1,\Sigma_0} \tag{3.45}$$

with $C_4=\frac{1}{6}$. Finally, we deduce the Lemma 3.1 norm with an order $1-s$. □

We recall the trace without proof (see [4] and in 2D [5]), the trace theorem lemma.

Lemma 3.2. *Let $\Omega\in\mathbb{R}^d$ with $d=2,3$ and D be a smooth subdomain of Ω. Let Σ_0 an open curve, Σ_e a smooth curve such that $\Sigma_0\cap\Sigma_e=\emptyset$, $\overline{\Sigma}_0\cup\overline{\Sigma}_e=\partial D$ the boundary. Let $(\mathcal{T}_h)_h$ be a regular family of triangulations, and V_h the associated P^1 finite element space. Then the trace operator γ_0 maps V_h into $H^1_{\Sigma_0}$ and one has*

$$|\gamma_0(v_h)|_{1,\Sigma_0}\leq\frac{C}{h^{1/2}}|v_h|_{1,\Omega}. \tag{3.46}$$

Then the approximation error is given in the following propositions.

Proposition 3.1. Let Ω be a domain of $\mathbb{R}^d$ with $d=3$ and $D\subset\subset\Omega$ a smooth subdomain with boundary ∂D. Let define Σ_0 an open curve, Σ_e a smooth curve such that $\Sigma_0\cap\Sigma_e=\emptyset$ and $\overline{\Sigma}_0\cup\overline{\Sigma}_e=\partial D$. Let $(\mathcal{T}_h)_h$ be regular family of triangulations with V_h the associated P_1 finite element space. Let $\varphi\in H^{-1/2+s}(\Sigma_0)$. Let $S_{\tilde{h}}$ be a family of quasi-uniform triangulation of $\partial D=\bigcup_i\Sigma_i$ and one denotes $\Sigma_{0,i}=\{\Sigma_i\,|\,\Sigma_i\in\Sigma_0\}$. Let $x_i\in\Sigma_i$, one defines

$$\varphi_h^{\tilde{h}}=\sum_{i=1}^{N_{\tilde{h}}}\lambda_i\delta_{x_i} \tag{3.47}$$

with the real coefficients λ_i define such that

$$\lambda_i=\langle\varphi,\mathbb{1}_{\Sigma_i}\rangle \tag{3.48}$$

the approximation. Then there exists a contant $C>0$ such that for all $v_h\in V_h$:

$$\left|\langle\varphi,v_h\rangle-\langle\varphi_h^{\tilde{h}},v_h\rangle\right|\leq C\sqrt{\frac{\tilde{h}}{h}}\tilde{h}^s\,|\varphi|_{-1/2+s,\Sigma_0}|v|_{1,\Omega}, \tag{3.49}$$

where $\langle\cdot,\cdot\rangle$ denotes the dual pairing for $H^{-1/2+s}(\Sigma_0)$ and $H^{1/2-s}(\Sigma_0)$.

Proof. From the Dirac source term definition, the interpolant is positive on Σ_0, then

$$\langle \varphi_h^{\tilde{h}}, v_h\rangle = \left\langle \sum_{i=1}^{N_{\tilde{h}}} \langle \varphi, \mathbb{1}_{\Sigma_i}\rangle \delta_{x_i}, v_h \right\rangle = \left\langle \sum_{i=1}^{N_{\tilde{h}}} \langle \varphi, \mathbb{1}_{\Sigma_{0,i}}\rangle, v_h(x_i) \right\rangle$$
$$= \sum_{i=1}^{N_{\tilde{h}}} \int_{\Sigma_{0,i}} \varphi v_h(x_i) = \left\langle \varphi, \sum_{i=1}^{N_{\tilde{h}}} v_h(x_i)\mathbb{1}_{\Sigma_{0,i}} \right\rangle. \tag{3.50}$$

If we consider the approximation error, one has

$$\left|\langle \varphi, v_h\rangle - \langle \varphi_h^{\tilde{h}}, v_h\rangle\right| = \left|\langle \varphi, v_h\rangle - \langle \varphi, \sum_{i=1}^{N_{\tilde{h}}} v_h(x_i)\mathbb{1}_{\Sigma_{0,i}}\rangle\right|$$
$$\leq \|\varphi\|_{H^{-1/2+s}(\Sigma_0)} \left\| v_h - \sum_{i=1}^{N_{\tilde{h}}} v_h(x_i)\mathbb{1}_{\Sigma_{0,i}}\rangle \right\|_{H^{1/2-s}(\Sigma_0)}$$
$$\leq \|\varphi\|_{H^{-1/2+s}(\Sigma_0)} \|v_h - v_{\tilde{h}}\|_{H^{1/2-s}(\Sigma_0)} \tag{3.51}$$

with the piecewise interpolant of v_h on Σ_0 such that

$$v_{\tilde{h}} = \sum_{i=1}^{N_{\tilde{h}}} v_h(x_i)\mathbb{1}_{\Sigma_{0,i}}. \tag{3.52}$$

Let denote $w_h^{\tilde{h}} = v_h - v_{\tilde{h}}$, then (3.31) gives the following majoration

$$\|w_{\tilde{h}}\|_{H^{1/2-s}}(\Sigma_0) \leq C\tilde{h}^{s+1/2}|v|_{1,\Sigma_0} \tag{3.53}$$

for $C>0$ adapted. Finally, using Lemma 3.2

$$\|w_{\tilde{h}}\|_{H^{1/2-s}}(\Sigma_0) \leq C\sqrt{\frac{\tilde{h}}{h}}\tilde{h}^s|v|_{1,\Omega}, \tag{3.54}$$

which ends the proof. □

To get the error for ϕ_x, we start with the Strang lemma

$$\|\phi_x - \phi_{x,h}\|_{H^1} \leq C\left(\inf_{v_h\in V_h}\|\phi_x - v_h\| + \sup_{w_h\in V_h}\left(\frac{|<\varphi, w_h> - <\varphi_h^{\tilde{h}}, w_{\tilde{h}}>|}{\|w_h\|}\right)\right). \tag{3.55}$$

We recall the Lemma 3.2 (Scott), the estimate (with $m=1$),

$$\|\phi_x - \phi_{x,h}\|_{H^r} \leq Ch^{1-r}\|\phi_x - \phi_{x,h}\|_{H^1}, \quad 0\leq r\leq 1. \tag{3.56}$$

We obtain from Proposition 3.1

$$\|\phi_x - \phi_{x,h}\|_{H^r} \leq Ch^{1-r}\left(\inf_{v_h\in V_h}\|\phi_x - v_h\| + \sqrt{\frac{\tilde{h}}{h}}\tilde{h}^s|\varphi|_{-1/2+s,\Sigma_0}\right). \tag{3.57}$$

If h and $\tilde{h}$ are of the same order, then we get

Proposition 3.2. We have the estimate, for $0\leq r\leq 1$ and $0\leq s\leq \frac{1}{2}$ and with P^1 finite element,

$$\|\phi_x-\phi_{x,h}\|_{H^r}\leq Ch^{1-r}\left(\inf_{\phi_{x,h}\in V_h}\|\phi_x-\phi_{x,h}\|+h^s|\varphi|_{-1/2+s,\Sigma_0}\right). \tag{3.58}$$

In particular for $d=2$ and in the extreme case $r=1$, if we assume $\phi_x\in H^2$, we obtain

$$\|\phi_x-\phi_{x,h}\|_{H^1}\leq C\left(\sqrt{h}\|\phi_x\|_{H^2}+h^s|\varphi|_{-1/2+s,\Sigma_0}\right), \tag{3.59}$$

we retrieve the result of [5]. However such regularity on ϕ_x seems too strong (Theorem 3.1). Moreover, for the case $d=3$, even with such regularity assumption a similar estimates

$$\inf_{v_h\in V_h}\|\phi_x-v_h\|_{H^1}\leq C\sqrt{h}\|\phi_x\|_2 \tag{3.60}$$

to the best of our knowledge, is not known.

In the case $0\leq r\leq \frac{1}{2}$ and without further assumption on ϕ_x than the Theorem 3.1,

$$\|\phi_x-\phi_{x,h}\|_{H^r}=O(h^{1-r}) \tag{3.61}$$

and the approximation of the source term is of higher order.

4 Numerical results

We implemented the forward problem (2.1) using a Finite Element Embedded Library in C++ www.feelpp.org (FEEL++) developed in our laboratory [10]. This library implements a framework for finite element methods based on the variational formulation with a language very close to the mathematical formulation. The implementation is parallel in a seamless manner for arbitrary dimensions and polynomial order thanks to the underlying features of the library. We highlight hereafter preliminary results for the diffusion problem with contact measurements. We propose a cross-verification with a former Matlab code and a validation by comparison with real measurements. An experimental instrument for small animal imaging was available [8] for performing time acquisitions on different test cases. We have at our disposal a set of measurements that has been acquired on homogeneous cylindrical objects made of plastic materials. The Impulse Response of the instrument is necessary to deconvolve the signal and to obtain the real measurement as a response to a Dirac pulse. However due to the detector sensitivity, the Impulse Response is difficult to obtain directly. Thus China Ink is used by instrumentalists as a medium in order to retrieve a signal which approximates the real Impulse Response. In practice, to perform comparison with physical measurements, our numerical solutions are convolved by the Impulse Response signal. The tests are performed on a cylindrical object with a radius of $20mm$. The dataset contains for each source 7 measurements corresponding to the $d\in[0,6]$ detectors dispatched regularly at the opposite location from the

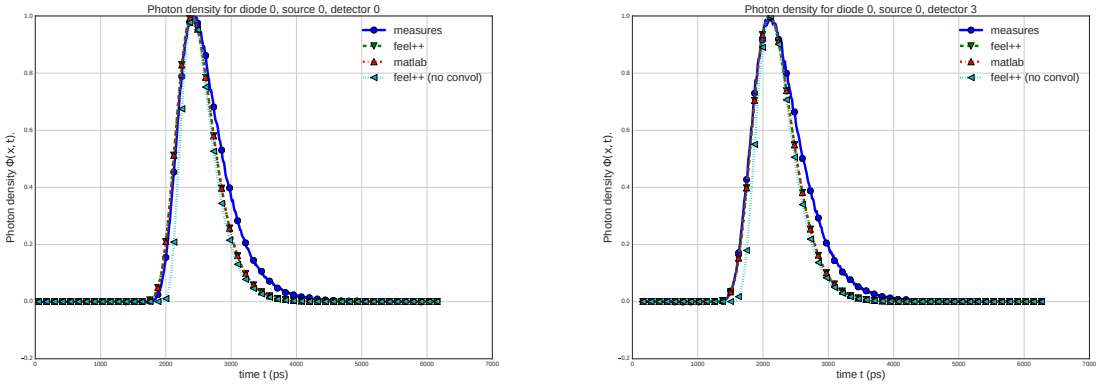

(a) Detector 0 (b) Detector 3

Figure 1: Diffusion simulation for $\mu_a = 0.006$ and $\mu_s' = 0.6$ on two detectors.

source. We have a total of 16 light sources taken from different angles. The built phantom has optical properties estimated $\mu_a = 0.006$ for the absorption and $\mu_s' = 0.6$ for the reduced scattering coefficient.

The Figure 1 shows cross-validated results with the former matlab code and compared with real measurements. Only 2 detectors for one source are presented in this paper, one located in the direct opposite position from the source $d = 3$. The second detector is located closer to the source $d = 0$. For comparison, numerical 1D results presented in the figure are readjusted with the exact signal time's grid by interpolation, then centred on the peak and finally normalized. We observe that the solution between the measurements $\Phi^k_{d,obs}(t)$ and the diffusion solutions $\Phi^k_x(x_d, t)$ for the source $k = 0$ and the d^{th} detector obtained with FEEL++ and the MathWorks Software (Matlab) match perfectly. These numerical solutions are convolved by the the Impulse Response Tissue Temporal Point Spread Function (TPSF) in order to compare with real data. The FEEL++ solution without convolution is displayed to highlight the effect of the Impulse Response on the peak slopes. Looking closely, the rising edge of our numerical solutions seems to match measurements, but it does not match for the falling edge. This difference can be interpreted in different ways. The most likely reason is that phantom optical properties μ_a, μ_s are not well estimated, for instance due to the complexity of creating perfectly homogeneous objects. In Figure 2, we have slightly modified the reduced scattering coefficient to reach $\mu_s' = 0.8$. By increasing this parameter, we can see that the curves match less at the beginning of the rising edge, but more on the falling one. The next natural step would consist in an optimization process to find the best suited input parameters μ_a, μ_s', thus consider the inverse problem.

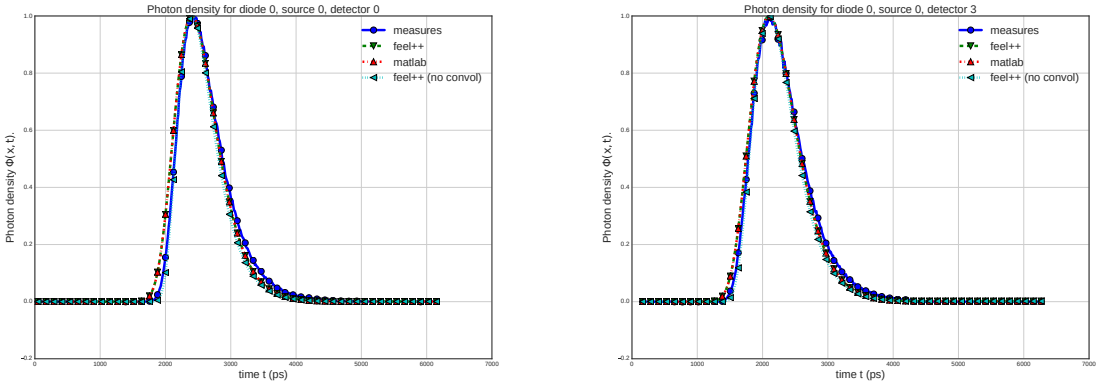

(a) Detector 0 (b) Detector 3

Figure 2: Diffusion simulation for $\mu_a = 0.006$ and $\mu_s' = 0.8$ on two detectors.

5 Conclusion

This paper presented a numerical analysis of the Diffuse Optical Tomography and Fluorescence (DOTF) problem. An analysis for both contact and non-contact measurements mode has been detailed for sources of Dirac's type. We proposed two strategies to handle the fluorescence coupling model equation (2.1) modelized by two diffusion equations. A first method consists in treating the convolution source term as a memory term, a second one consists to introduce a new ODE that can be solved explicitly. A finite element approach has been considered to handle the numerical aspects. Convergence results have been proposed to distinguish the two measurement modes presented in first sections. Finally, preliminary numerical results have been proposed to verify the mathematical model and the implementation based on a C++ parallel framework for FEM. The comparison with real measurements presented in this paper highlights the difficulty to find proper optical parameters in order to fit the data. Thus, as a perspective and future work, the inverse problem shall be considered in order to identify both fluorescence and diffusion parameters.

References

[1] S.R Arridge. Optical tomography in medical imaging, IOPScience Inverse problem, 15(2), 1999.

[2] Philippe Benilan and Haim Brezis. Solutions faibles d'équations d'évolution dans les espaces de hilbert. In Annales de l'institut Fourier, volume 22, pages 311-329, 1972.

[3] Lucio Boccardo and Thierry Gallouët. Non-linear elliptic and parabolic equations involving measure data. Journal of Functional Analysis, 87(1):149-169, 1989.

[4] Guillaume Dollé. Diffuse optical tomography and fluorescence for tumour detection. Theses, Université de Strasbourg, September 2018.
[5] Benoit Fabrèges and Bertrand Maury. Approximation of single layer distributions by dirac masses in finite element computations. Journal of Scientific Computing, 58(1):25-40, 2014.
[6] Olga Aleksandrovna Ladyzhenskaia, Vsevolod Alekseevich Solonnikov, and Nina N Ural'ceva. Linear and quasi-linear equations of parabolic type, volume 23. American Mathematical Soc., 1968.
[7] Jacques Louis Lions and Enrico Magenes. Non-homogeneous boundary value problems and applications, volume 1. Springer Science & Business Media, 2012.
[8] Bruno Montcel and Patrick Poulet. An instrument for small-animal imaging using time-resolved diffuse and fluorescence optical methods. Nuclear Instruments and Methods in Physics Research, A 569, 2006.
[9] Farouk Nouizi. Tomographie optique diffuse et de fluorescence préclinique : instrumentation sans contact, modélisation et reconstruction 3D résolue en temps. PhD thesis, Université de Strasbourg, 2011.
[10] Christophe Prud'Homme, Vincent Chabannes, Vincent Doyeux, Mourad Ismail, Abdoulaye Samake, and Gonçalo Pena. Feel++: A computational framework for galerkin methods and advanced numerical methods. In ESAIM: Proceedings, volume 38, pages 429–455. EDP Sciences, 2012.
[11] Ridgway Scott. Finite element convergence for singular data. Numerische Mathematik, 21(4):317-327, 1973.
[12] Guido Stampacchia. Le problème de dirichlet pour les équations elliptiques du second ordre à coefficients discontinus. In Annales de l'institut Fourier, volume 15, pages 189-257. Institut Fourier, 1965.
[13] Murielle Torregrossa. Reconstruction d'images obtenues par tomographie optique dans le proche infrarouge. PhD thesis, Université de Strasbourg, 2003.
[14] Y. Yamada and S. Okawa. Diffuse optical tomography: Present status and its future. Optical Review, 21(3):185-205, 2014.